**IJCRT.ORG** 

ISSN: 2320-2882



# INTERNATIONAL JOURNAL OF CREATIVE RESEARCH THOUGHTS (IJCRT)

An International Open Access, Peer-reviewed, Refereed Journal

# Effect Of Biosynthesized And Poultry Waste Synthesized Fe Nanoparticles On Degradation Of Amikacin Antibiotic

<sup>1</sup>Mathivanan Varatharajan, <sup>2\*</sup>Murugesan Kumarasamy, <sup>3</sup>Siddharth Sampathkumar, <sup>1</sup>Research Scholar, Department of Environmental Science, Periyar University, Salem – 636011, Tamil Nadu, India

<sup>2\*</sup>Professor, Department of Environmental Science, Periyar University, Salem – 636011, Tamil Nadu, India
<sup>3</sup>Associate Professor, Department of Mechanical Engineering, PSN College of Engineering & Technology, Melathediyoor, Tirunelveli – 627152, Tamil Nadu, India

Abstract: In this manuscript, iron nanoparticles (FeNPs) were successfully used for degrading the amikacin antibiotic. For degrading amikacin, Ficus hispida (F. hispida) bio-extract and poultry biowaste were used for stabilizing the synthesis of Fe nanoparticles. The effectiveness of the Fe nanoparticles prepared by using both methods was compared for their effectiveness in degrading Fe nanoparticles. FeNPs were created, and their properties were measured using UV-Vis spectroscopy, FTIR, XRD The appropriateness of sunlight for the degradation experiments was assessed. Different experimental variables, including initial concentration of the antibiotic, initial dose of FeNPs, reaction time, ionic strength of the solution, and pH of the solution, were researched. The conclusion was that a mixture of sunlight with poultry biowaste-synthesized FeNPs had a high level of degradation efficacy in comparison with F. hispida-synthesized FeNPs. The production of FeNPs and their application in amikacin degradation using poultry biowaste provide a sustainable source for synthesis, promote waste valorization, and contribute to the development of a circular economy.

Index Terms - poultry biowaste extract, Fe nanoparticles, amikacin, antibiotic degradation, anti-bacterial assay

#### I. Introduction

Antibiotics are known to be the twentieth century miracle drugs that have revolutionized the medical industry to the next level by saving many lives and morbidities caused by bacterial infections by large margins. However, their extensive and often indiscriminate usage has resulted in a growing environmental disaster. The widespread use of antibiotics in the environment poses serious hazards, including the growth of antibiotic-resistant bacteria and the disturbance of microbial ecosystems. The recent literature has highlighted the escalating issue of antibiotics penetrating the environment, particularly through agricultural discharge, drug waste, and lack of adequate treatment of the wastewater. Recent research conducted by Zhao et al. (2023) on the presence of antibiotics in surface waters in the surroundings of agricultural facilities found alarming results of their presence in the waters [1]. In the same manner, Gwenzi et al. (2023) have extensively researched the disposal of pharmaceutical waste and have found out that improper disposal procedures are a major cause of environmental pollution, which in turn exacerbates the risk of resistant infections [2].

The decomposition and detoxification of the antibiotics in the environment play a vital role in reduction of adverse impacts of the antibiotics. According to Manikandan et al. (2023), biochar can be used to adsorb and degrade various antibiotics, which is a lasting and cost-efficient solution [3]. Furthermore, Kumari and Das (2023) examined the application of enzymatic degradation, which combines naturally occurring enzymes to degrade the antibiotic substances, as one of the potential methods of decontaminating polluted areas [4]. The modern detoxifying approaches have enormous potential in fighting antibiotic toxicity. Heris et al. (2023) also examined the potential of photocatalysis performed using Titanium oxide (TiO2)

IJCRT2510209 International Journal of Creative Research Thoughts (IJCRT) www.ijcrt.org b703

nanoparticles and the findings demonstrated that the high-order antibiotic breakdown occurs under UV light after the use of hydroxyl radicals [5]. In addition, the article by Khan et al. (2022) examined the potential of Fenton-type reactions and other advanced oxidation processes (AOPs) that effectively degrade antibiotic compounds by using hydroxyl radicals [6]. Vinayagam et al. [7] have emphasized the usage of electric chemistry oxidation which supports the reduction of the pollutants with the help of electric current, which is effective and scalable.

Within the past few years, nanoparticles have been discovered as efficient antibiotic detoxification substances due to their peculiarities and high reactivity. The researchers of Khan et al. (2023) examined the effectiveness of silver nanoparticles (AgNPs) in degrading various antibiotics, pointing out that it may destroy bacterial cell walls and accelerate the degradation of antibiotics [8]. Another research by Sun et al. (2023) focused on the application of iron oxide nanoparticles (Fe3O4NPs), and it showed the possibility of using this catalyst to facilitate the degradation process through Fenton-like reactions [9]. The synthesis of nanoparticles has increased the application of the nanoparticles in the field of environmental decontamination. The green synthesis method of producing ZnO nanoparticles using plant extracts mentioned by Alprol et al. (2023) reduces pollution to the environment as well as enhances detoxification [10]. Yang et al. (2023) also developed a new hydrothermal synthesis method to obtain highly porous silica nanoparticles with the highest surface area and reactivity in breaking antibiotics [11]. The batch studies have given significant knowledge on the way of practicing the detoxifying technologies in the open natural sunlight. The efficacy of photocatalysis of ZnO nanoparticles driven by solar energy was determined by Dhiman and Kondal (2023) in degrading antibiotics in water samples [12]. Also, the review of the literature demonstrated that there is a lack of studies on the disinfection of antibiotics on the basis of biosynthesized nanoparticles, as well as that large-scale projects on the use of solar energy in the process of detoxification are a viable option [13] [14] [15]. Utilizing poultry biowaste as a catalyst for the synthesis of Fe nanoparticles (FeNPs) is a novel eco-friendly approach. The synthesized FeNPs are evaluated its effective degradation of antibiotics, especially with amikacin. Thus, the current study focused on the novel and ecofriendly utilization of poultry biowaste as a catalyst and coating agents for the synthesis of FeNPs, which exhibits the effective degradation of antibiotics, thereby favoring environmental sustainability and the circular economy.

#### II. MATERIALS & METHODS

# 2.1 Chemicals and extract preparation

The substances employed in this study included ferrous sulphate heptahydrate (99.9% pure) and sodium borohydride (Tata Chemicals, India). Hydrochloric acid and sodium hydroxide were bought from Indian Scientific Supplies, India, while the antibiotic compound Amikacin (Amikacin sulphate) was procured from Ranbaxy Laboratories, India. All chemicals used were of high purity and industrial grade quality; hence they were used directly without any further purification. Poultry biowaste and *F. hispida* extract were used for synthesis of FeNPs. To prepare the poultry biowaste extract for FeNPs synthesis, poultry biowaste was first collected from local market and thoroughly cleaned to remove pollutants. It was then dried at 100°C to eliminatemoisture content. The dried waste was ground into a fine powder using a mortar and pestle, and this powder was sieved to ensure consistent particle size, making it suitable for subsequent processing in the synthesis of FeNPs. For the preparation of *F. hispida* extract, fresh leaves were gathered, properly washed, and air-dried. The dried leaves were then ground to a fine powder. In order to extract the bioactive compounds, 75 g of poultry waste and *F. hispida* powder was separately heated in 500 ml of distilled water for 30 minutes. Then, it was filtered through Whatman No 1 filter paper to eliminate solid residues, and the resulting filtrate served as the bio-extract in the synthesis process.

# 2.2 Synthesis of FeNPs using Poultry biowaste extract and F. hispida extract

A wet chemical process was used to synthesize FeNPs from poultry biowaste and *F. hispida* extract. To 50 ml of each extract, 1.39 g of ferrous sulphate heptahydrate was added and stirred for 15 minutes at 350 rpm. Simultaneously, 2.3 g of sodium borohydride was dissolved in 200 ml of deionized water (pH 6), stirred until completely dissolved, and cooled in an ice bath. Once approaching freezing temperature, the bio-extract-ferrous sulphate solutions were added to the sodium borohydride solution and aggressively swirled at 1000 rpm until both were well combined. The nanoparticles were vigorously rotated at 8000 rpm for 15 minutes, then separated using neodymium magnets, washed with acetone, and vacuum-dried for 12

hours. To avoid contamination, the produced nanoparticles were maintained in air tight vials kept in a desiccator at ambient temperatures.

# 2.3 Characterization of the poultry waste and synthesized FeNPs

UV-Vis spectrophotometer was used to check the optical characteristics and confirm the formation of FeNPs. The sample was scanned from 200 to 800 nm to record the characteristics absorption peak. Fourier transform infrared spectroscopy (FTIR) was employed to identify the functional groups in the poultry waste extract and F. hispida extract and their role in the formation of FeNPs. The poultry waste extract, F. hispida extract and synthesized FeNPs was mixed with KBr and scanned in the range of 4000-400 cm<sup>-1</sup>. X-ray diffraction (XRD) was employed to determine the crystalline nature of the FeNPs. The FeNPs samples were scanned in the  $2\theta$  range of 10- $80^{\circ}$  using Cu K $\alpha$  radiation and the pattern was compared with standard JCPDS data.

#### 2.4 Batch studies

Using sterilized glass beakers, degradation experiments were conducted in sterilized glass beakers, divided into two batches. The first batch utilizedFeNPsfrom poultry waste, while the second batch utilized FeNPs synthesized from *F. hispida* extract. Amikacin solutions of different concentrations were prepared using deionized water. Amikacin sulphate solution (30 ml) was mixed with FeNPs and subjected to ultrasonic agitation for 45 min. The amikacin degradation efficiency was evaluated by measuring the reduction in antibiotic concentration. Comparative analysis was done to evaluate the degradation efficiency of FeNPs frompoultry biowaste and synthesized FeNPs from *F. hispida*. At different antibiotic concentrations, FeNPs quantity, solution pH, ionic strength and reaction duration, the antibiotic degradation efficiency was calculated. The following equation was used for calculating the antibiotic degradation efficiency was as follows:

Degradation effeciency % = 
$$\frac{C_o - C}{C_o} x 100$$

In the equation above, C<sub>0</sub> represents the original concentration and C<sub>t</sub> represents the concentration over time. The absorbance variations were measured using a UV-Vis spectrophotometer. The pH of FeNPs with amikacin solution was adjusted using sodium hydroxide and sulfuric acid. To test the ionic strength, amikacin solution was mixed with NaCl and FeNPs. The concentration of NaCl was increased from 0.05M to 0.1M, resulting in variations in antibiotic degradation efficiency. The concentration of residual amikacin following degradation was determined using a UV-Vis spectrometer. FeNPs were isolated and removed from solution using neodymium magnets.

#### 2.5 Residual antibiotic activity studies

After studying the breakdown of amikacin using FeNPs, residual antibiotic activity was evaluated on *Escherichia coli* (ATCC 8739) (*E. coli*) as a test microorganism. From the stock of *E.coli*, an entire loop was taken and inoculated into 5 ml of sterile nutrient broth. After incubated for 18-24 hours at 37°C, the residual antibacterial assay was done using the agar-well diffusion method. 100 μl of the inoculum (1.5×10<sup>8</sup> CFU/ml) was inoculated with Mueller Hinton Agar media poured Petri plates. The treated antibiotic solution was filtered to eliminate nanoparticles and was added into well made in the plate, which was incubated overnight at 37°C. The measuring the diameter of the zone of inhibition observed after treating with the filtered solution indicates the presence of residual antibiotic action, whereas a lack of growth inhibition demonstrated the antibiotic had been successfully degraded. This method helps to confirm the degrading process's efficacy.

#### III. RESULTS &D DISCUSSIONS

#### 3.1. Synthesis of FeNPs using poultry waste

FeNPs were synthesized using poultry biowaste, which included feathers, eggshells, dung, blood, bones and fat. This trash, which is frequently viewed as an environmental burden, offers a sustainable and eco-friendly method of nanoparticle production. The biowaste comprised organic components including proteins, amino acids, keratin and other organic chemicals facilitated the reduction of Fe<sup>3+</sup> to Fe<sup>0</sup>, while blood and bones supplied iron [14, 15, 16]. The biowastematerialwas treated thermally and chemically to

eliminate impurities, including residual antibiotics, ensuring pollutant free FeNPs[16]. The resulting nanoparticles have potent adsorption and degradation properties against pollutants such as amikacin and were extremely reactive. By minimizing the use of hazardous chemicals and lowering environmental contamination, this strategy not only reduced agricultural waste but also promoted green chemistry [17].

#### 3.1 Calibration curve of amikacin

Various concentration of amikacin (20, 40, 60, 80, and 100 ppm) was subjected to UV-Vis analysis and the variations in spectral peaks are shown in Figure 1. For reducing errors during experimental process, the experiments were conducted in triplicate and the average of the triplicate was recorded. From Figure 1, the variations in peaks were found near 400 nm and 570 nm. The linearity plot for amikacin UV-Vis peaks near 400 nm and near 570 nm is shown in Figure 2 (a) and Figure 2 (b), respectively. According to Figure 2 (a), the UV-Vis spectra of amikacin revealed a clear linear connection between concentration and absorbance at 400 nm, which was compatible with Beer's Law. The data showed that as the quantity of amikacin grew from 20 to 100 ppm, the absorbance values at 400 nm increased correspondingly. At 20 ppm, the absorbance was 0.09235; at 40 ppm, it increased to 0.187. Increase in concentration to 60 ppm, 80 ppm, and 100 ppm produced absorbance values of 0.26776, 0.36474, and 0.5309, respectively [18]. Based on Figure 2 (b), the UV-Vis spectra of amikacin revealed a clear linear connection between concentration and absorbance at 570 nm. The data showed that when the quantity of amikacin increased from 20 to 100 ppm, the absorbance values at 570 nm increased proportionately. At 20 ppm, the absorbance was 0.0694; at 40 ppm, it increased to 0.14678. Further concentration increases to 60 ppm, 80 ppm, and 100 ppm yielded absorbance values of 0.21023, 0.28163, and 0.4105, respectively [19]. The linear increase in absorbance with concentration demonstrated that the solution followed Beer's Law within this concentration range. The linearity of the absorbance data indicated that the molar absorptivity (\(\epsilon\)) was constant across the tested concentrations. This consistency showed that the amikacin molecules in solution did not experience significant aggregation, interaction, or chemical changes that would impair their capacity to absorb light at 400 nm within the provided concentration range.

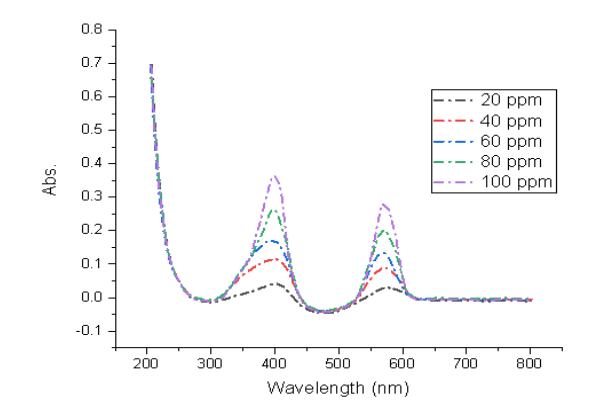


Figure 1. UV-Vis spectrum of amikacin at different concentrations.

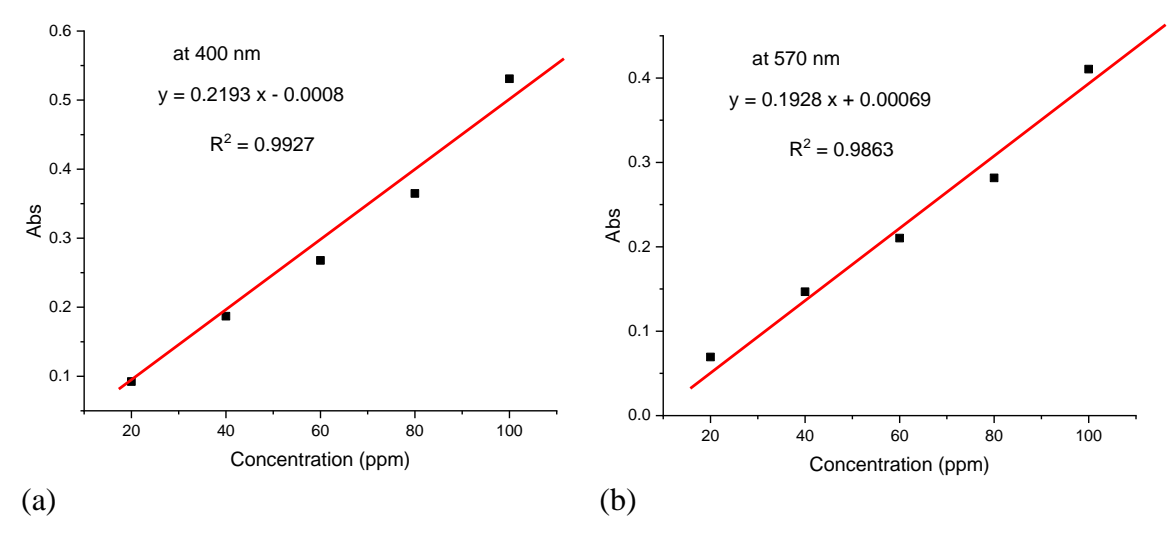


Figure 2. Linearity plot for amikacin UV-Vis at (a) 400 nm and (b) 570 nm.

The proportional increase in absorbance with concentration ensured that the solution was dilute enough to minimize deviations from linearity at higher concentrations caused by intermolecular interactions or restrictions in the detector's linear response range [21] [22]. This allows the quantification of the amikacin concentration in degradation experiments using UV-Vis spectrophotometer.

#### 3.2 Characterization of FeNPs

UV-Vis spectrum of poultry biowaste synthesized FeNPs and *F. hispida* bio-synthesized FeNPs are shown in Figure 3 (a) and Figure 3 (b), respectively. The UV-Vis spectra study revealed unique properties for FeNPs synthesized from poultry biowaste and *F. hispida*. Figure 3 (a) shows that the FeNPs synthesized from poultry biowaste had strong absorption peaks at 256.3 nm and 323.47 nm. These peaks indicate the presence of FeNPs and their surface plasmon resonance, implying effective nanoparticle production [23]. In contrast, Figure 3 (b) indicates that FeNPs derived from *F. hispida* had absorption peaks at 239.32 nm and 342.72 nm. The modifications in peak positions between the two sources highlight particle size, shape, and capping agents, all of which have an impact on the optical characteristics and stability of the nanoparticles [24]. This is because the UV-VIS absorption peaks of the two sources have differences indicating that the properties of the nanoparticles are different due to the different ways of synthesizing them and the natural capping agents. The results of these studies highlight the relevance of source material and synthesis mechanism in furnishing the optical and structural characteristics of FeNPs [25].

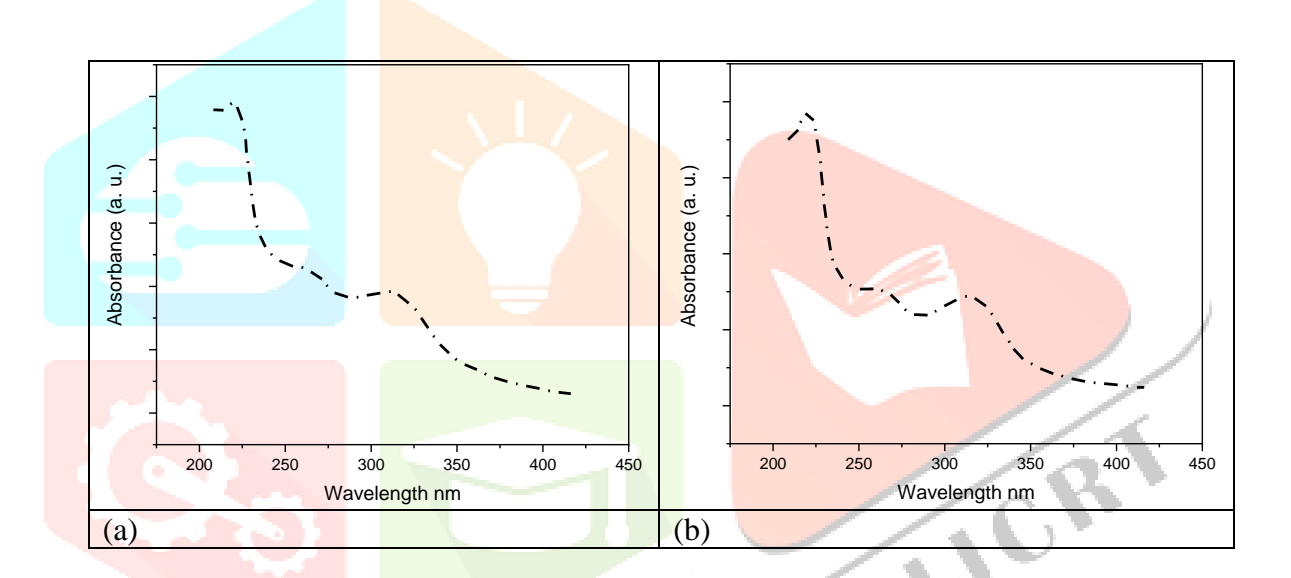
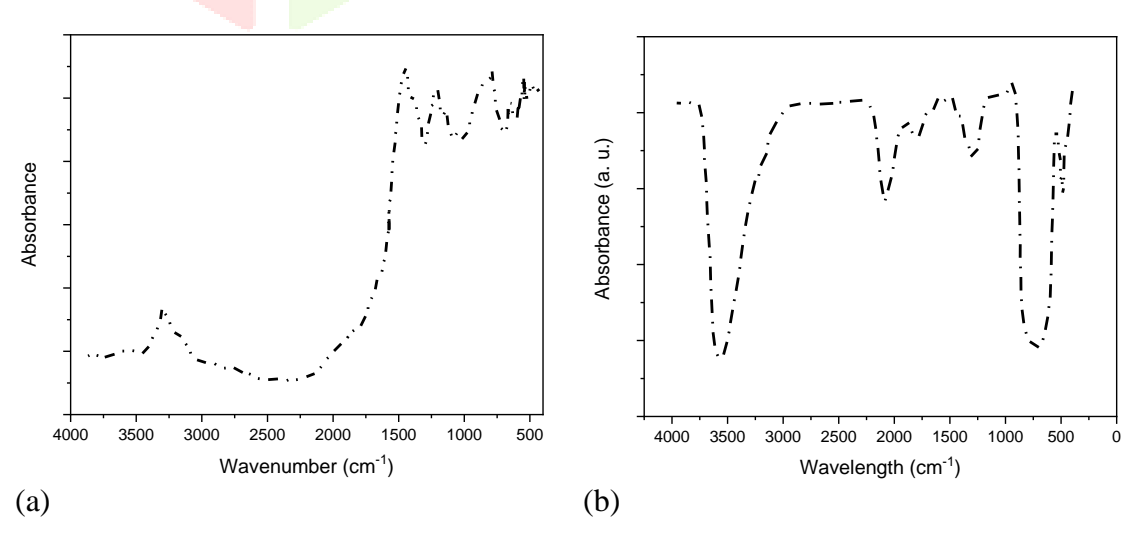


Figure 3. UV-Vis spectrum of (a) poultry biowaste synthesized FeNPs, and (b) *F. hispida* synthesized FeNPs.



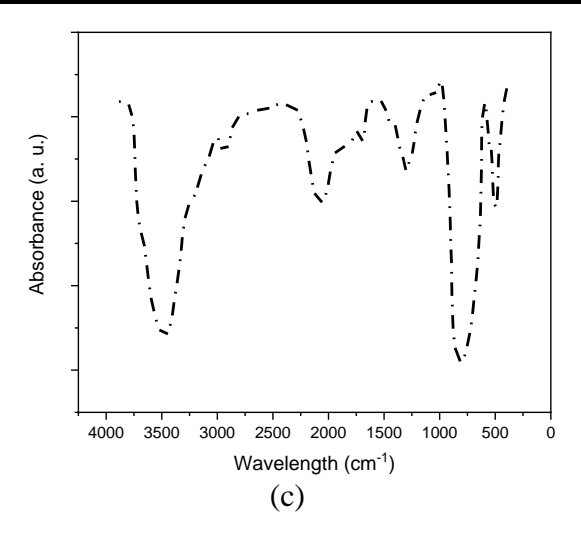


Figure 4 FTIR spectrum of (a) Poultry waste extract and (b) poultry biowaste synthesised FeNPs, (c) *F. hispida* synthesized FeNPs.

Figure 4 (a), Figure 4 (b) and Figure 4 (c) demonstrate FTIR spectrum of poultry biowaste, poultry biowaste synthesized FeNPs and F. hispida bio-synthesized FeNPs, respectively. The FTIR analysis of poultry waste showed distinct peaks at 3302 and 3398 cm<sup>-1</sup> correspond to N-H stretching, likely from amines or proteins. Peaks around 3559, 3742, and 3703 cm<sup>-1</sup> are attributed to O-H stretching, indicating the presence of hydroxyl groups from water. The peaks at 3221, 3446, and 3653 cm<sup>-1</sup> suggest hydrogen bonding interactions or stretching vibrations of amides. These functional groups confirm the presence of proteins, amino acids, and other organic compounds crucial for nanoparticle stabilization. Protein is the most abundant component in poultry biowaste, including keratin, collagen, and other fibrous proteins. These proteins are plentiful in feathers, skin, and connective tissues. Biowaste also contains considerable amounts of amino acids, lipids, and minerals derived from bones, such as calcium and phosphorus.

Due to its high protein content, poultry biowaste proves to be an excellent source of natural reducing and stabilizing agent for FeNPs synthesis [26]. Figure 4b of the FTIR spectra of FeNPs synthesized by poultry waste indicates the presence of prominent absorption bands that represent various functional groups and bonding interactions. Vibrations ranging between 525-937cm<sup>-1</sup> also indicate the generation of FeNPs [27]. The C-H bending at the peak of 1457 cm<sup>-1</sup> and C=O stretching vibrations at 1842 cm<sup>-1</sup> respectively show the presence of organic molecules. The absorption at 2267 cm 2267 cm 2267 cm<sup>-1</sup> C N stretching and 2569 cm<sup>-1</sup> S H stretching vibrations, respectively, indicate the presence of Sulphur-containing compounds. The presence of hydroxyl groups is indicated by the presence of large O-H stretching at 3649 cm<sup>-1</sup>, which is the cause of the stability and dispersibility of the nanoparticles [28]. The FTIR spectrum of *F. hispida* synthesized FeNPs (Figure 4c) displays diverse peaks indicating various functional groups and bonding interactions. The peak at 439 cm<sup>-1</sup> and stretching vibrations from 533 cm<sup>-1</sup> to 869 cm<sup>-1</sup> indicate the production of FeNPs. The modest peak at 1439 cm<sup>-1</sup> indicates the existence of C-H bending vibrations, indicating organic remnants from the bio extract. The signal at 2123 cm<sup>-1</sup> represents C=N stretching, indicating the presence of nitrile groups. The broad stretching vibration at 3512 cm<sup>-1</sup> is due to O-H stretching, which indicates hydroxyl groups [29].

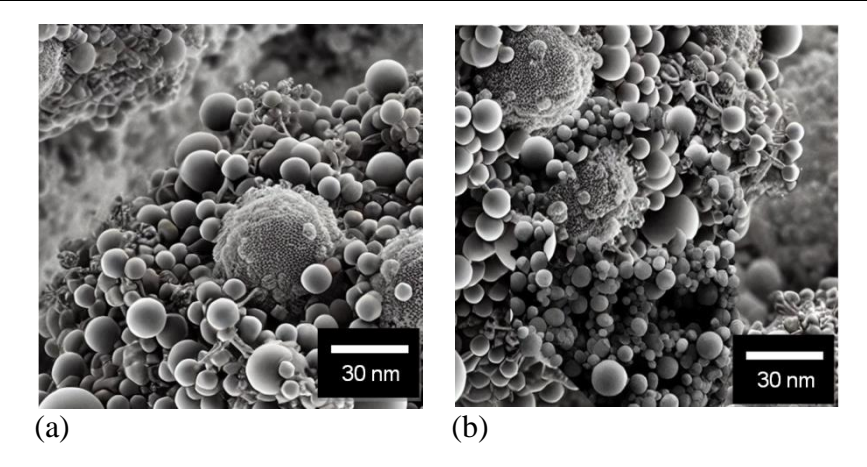


Figure 5. FE-SEM image of (a) poultry biowaste synthesized FeNPs, (b) F. hispida synthesized FeNPs.

Field Emission Scanning Electron Microscopy (FE-SEM) image of FeNPs synthesized using poultry biowaste and F. hispida is shown in Figure 5 (a and b). The FE-SEM image of FeNPs synthesized using poultry biowaste (Figure 5a) shows spherical nanoparticles with a uniform distribution and an average size between 13 to 23 nm.

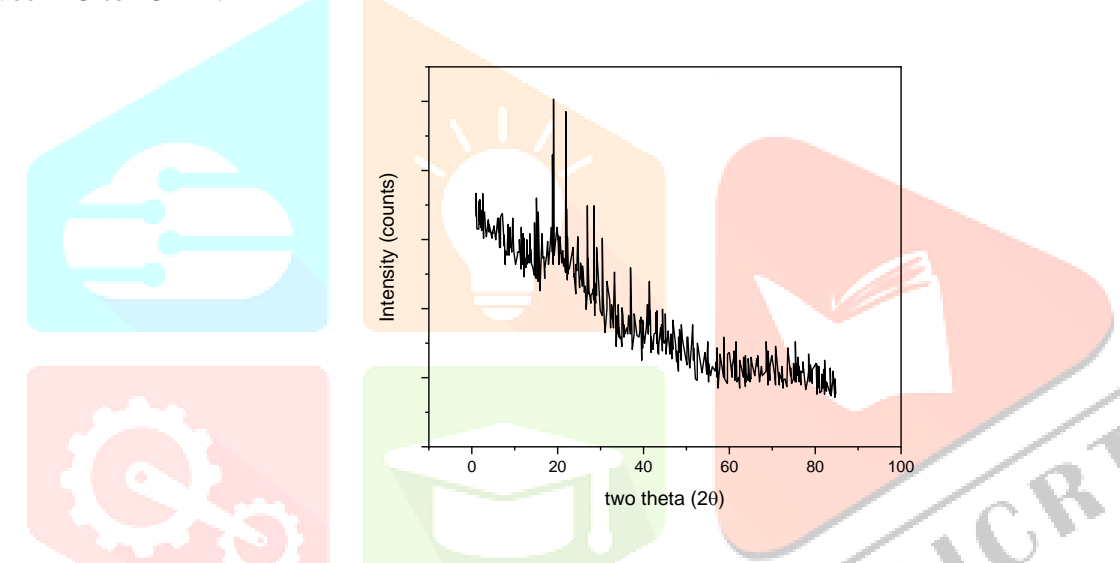


Figure 6. XRD image of FeNPs synthesized using poultry biowaste extract.

The particles appear well-dispersed, indicating good stability. In contrast, the FE-SEM image of FeNPssynthesized using F. hispida (Figure 5b) reveals slightly larger, irregularly shaped nanoparticles with some agglomeration [30]. The size distribution suggests greater variability in morphology and surface characteristics. The nano size of FeNPs was determined using FE-SEM, which allowed for high-resolution imaging of the particles' surface morphology. The diameters varied from 13 to 23 nm, confirming the nanoscale dimensions [31]. XRD spectra of FeNPs synthesized using poultry biowaste is shown in Figure 6.The XRD graph of FeNPssynthesized utilizing poultry biowaste revealed different peaks matching to iron's crystalline structure, typically at 2θ values of roughly 30°, 35°, 43°, 53°, and 57°. These peaks represented the face-centered cubic (FCC) structure of FeNPs. The sharpness of the peaks indicated strong crystallinity, whilst the intensity and location of the peaks indicated successful synthesis. Furthermore, a modest broadening of peaks may indicate a drop-in particle size, which is typical of nanoscale materials [32]. GC-MS studies on poultry biowaste extract is shown in Figure 7 and the retention times of organic compounds present in poultry biowaste extract are presented in Table 1.The GC-MS analysis of poultry biowaste extract revealed multiple peaks corresponding to various organic compounds. Key bioactive compounds like oleic acid and palmitic acid were also detected at retention times of 9.75 and 8.92 minutes, respectively, indicating the presence of organic compounds involved in nanoparticle surface modification and bioactivity [33].

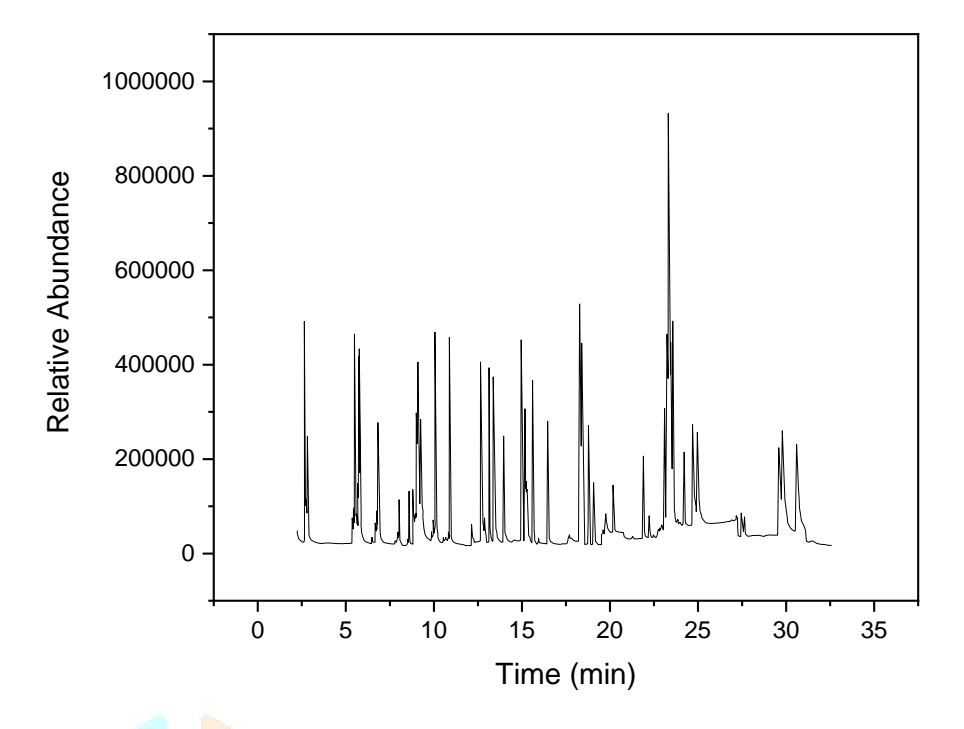


Figure 7. GC-MS spectrum of poultry biowaste synthesized FeNPs.

Table 1. GC-MS analysis of poultry biowaste extract.

No.	Compound IUPAC	Rt (min)	Target ion (m/z)	Qualifier ion 1 (m/z)	Qualifier ion 2 (m/z)
1	Indole	5.10	117	118 (70)	115 (50)
2	Skatole (3-methylindole)	5.55	131	132 (75)	129 (60)
3	Phenol	5.35	94	95 (60)	93 (40)
4	p-Cresol	6.25	108	107 (65)	109 (55)
5	Palmitic acid	8.92	256	255 (80)	258 (65)
6	Oleic acid	9.75	282	281 (75)	283 (60)
7	Ammonia (NH <sub>3</sub> )	4.02	17	16 (85)	18 (50)
8	Hydrogen sulfide (H <sub>2</sub> S)	3.85	34	33 (75)	35 (55)
9	Methanethiol	4.35	48	47 (65)	49 (45)
10	Trimethylamine	4.55	59	58 (70)	60 (50)
11	Butanoic acid (Butyric acid	l) 6.45	88	87 (65)	89 (50)
12	Putrescine (1,4-diaminobutane)	6.95	88	89 (70)	87 (60)
12	Cadaverine (1,5-diaminopentane)	7.15	101	102 (75)	100 (60)
14	Limonene	9.40	136	137 (80)	135 (60)
15	Dodecane	9.75	170	171 (85)	169 (55)
16	Hexadecane	10.45	226	227 (80)	225 (60)

#### 3.3 Batch antibiotic degradation studies

# 3.3.1. Changes in amikacin antibiotic degradation efficiency at various dosage of FeNPs

In the degradation experiments of amikacin antibiotic using FeNPs, four different conditions were compared: poultry biowaste synthesized FeNPs in the dark, in sunlight, *F. hispida* synthesized FeNPs in the dark, and sunlight. The amikacin concentration was constant at 180 mg/l, with reaction duration of 235 minutes, an ionic strength of 0.08 M, and a pH of 8. The variations in degradation efficiencies at different FeNPs quantity are shown in Figure 8.

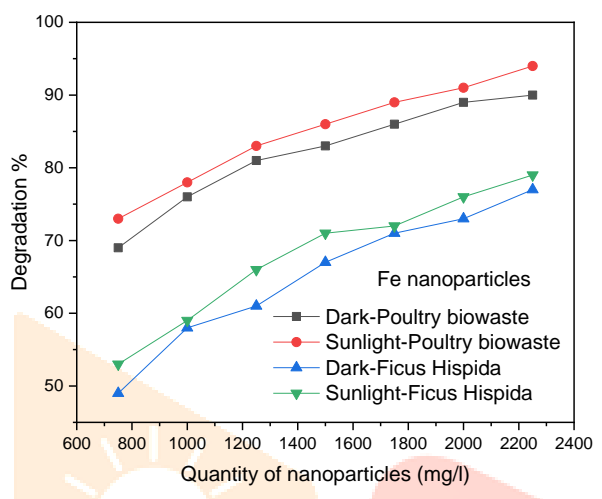


Figure 8. The variations in degradation efficiencies at different FeNPs quantity.

At a nanoparticle dosage of 750 mg/l, the degradation efficiency using poultry biowaste synthesized FeNPs was 69% in the dark and 73% in sunlight, while *F. hispida* synthesized FeNPs showed efficiencies of 49% in the dark and 53% in sunlight. As the dosage increased to 1500 mg/l, poultry biowaste derived nanoparticles achieved efficiencies of 83% in the dark and 86% in sunlight, compared to 67% and 71% degradation observed in dark and sunlight, respectively for *F. hispida* derived nanoparticles [34]. At a higher dosage of 2000 mg/l, the efficiency for poultry biowaste nanoparticles reached 89% in the dark and 91% in sunlight, whereas *F.hispida* nanoparticles showed 73% in the dark and 76% in sunlight. At the maximum dosage of 2250 mg/l, the efficiencies were 90% in the dark and 94% in sunlight for poultry biowaste nanoparticles, and 77% in the dark and 79% in sunlight for *F. hispida* nanoparticles [35].

#### 3.2.2 Changes in amikacin degradation efficiency at various initial amikacin concentrations

In the degradation experiments, the nanoparticle concentration was kept constant at 1500 mg/l, with reaction duration of 235 minutes, an ionic strength of 0.08 M, and a pH of 8. The variations in degradation efficiencies at different Amikacin concentrations are shown in Figure 9. At an initial concentration of 120 mg/l, the degradation efficiencies were 83 % in the dark and 93% in sunlight for poultry biowaste synthesized FeNPs, as compared to 69% in the dark and 79% in sunlight for *F. hispida* synthesized FeNPs. As the initial concentration increased to 200 mg/l, the degradation efficiency dropped to 68% in the dark and 78% in sunlight for poultry biowaste nanoparticles, while it decreased to 57% in the dark and 61% in sunlight for *F. hispida* nanoparticles [36]. At the highest concentration of 220 mg/l, the efficiencies further declined to 59% in the dark and 66% in sunlight for poultry biowaste nanoparticles, and 47% in the dark and 52% in sunlight for *F. hispida* nanoparticles [37].

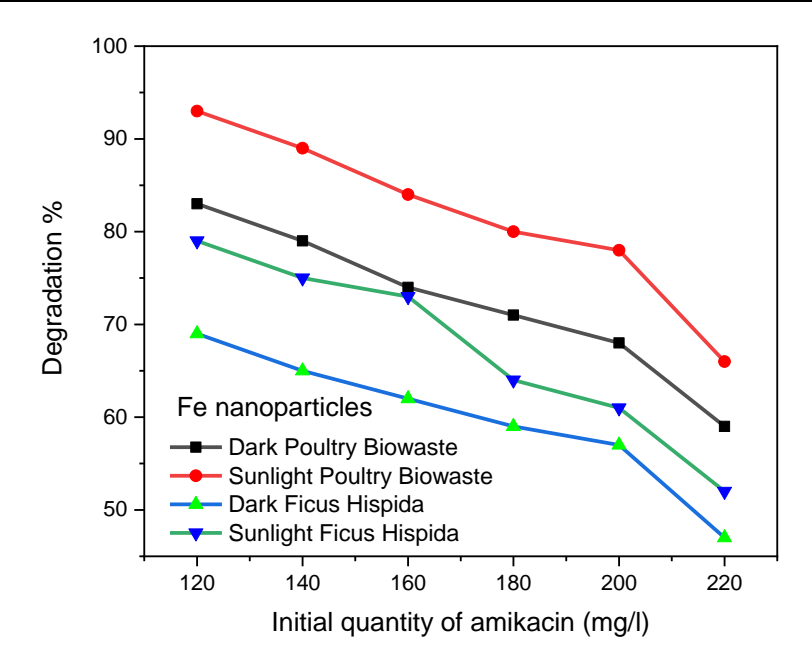


Figure 9. Variations in degradation efficiencies at different concentrations of amikacin.

#### 3.2.3 Changes in amikacin antibiotic degradation efficiency at various reaction duration

In the degradation experiments, the concentration of nanoparticles was constant at 1500 mg/l, with an amikacin sulphate concentration of 180 mg/l, ionic strength of 0.08 M, and pH of 8. Changes in amikacin antibiotic degradation efficiency at various time intervals are shown in Figure 10. At 145 minutes, poultry biowaste FeNPs showed the degradation efficiencies were 53% (dark) and 55% (sunlight), while *F. hispida* FeNP showed 42% (dark) and 51% (sunlight). At 235 minutes, the degradation efficiency for poultry biowaste FeNPs rose to 71% (dark) and 74% (sunlight), compared to 63% (dark) and 68% (sunlight) for *F. hispida* nanoparticles [38]. At 295 minutes, the efficiency was 83% (dark) and 88%(sunlight) for poultry biowaste nanoparticles, whereas *F. hispida* nanoparticles achieved 74% (dark) and 79% (sunlight) [39]. At the longest duration of 325 minutes, the efficiencies reached 89% (dark) and 92% (sunlight) for poultry biowaste nanoparticles, and 79% (dark) and 83% (sunlight) for *F. hispida* nanoparticles.

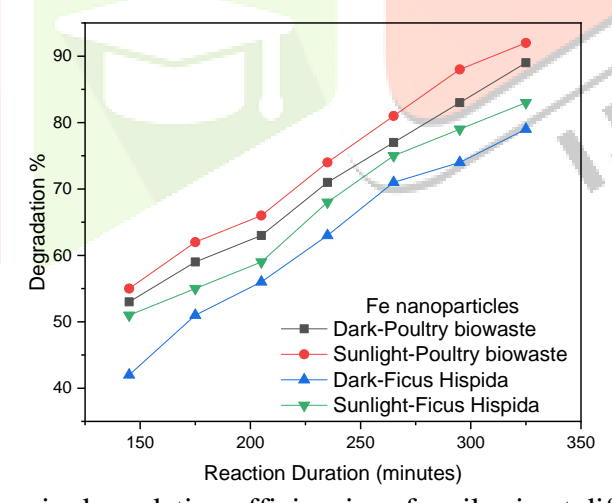


Figure 10. Variations in degradation efficiencies of amikacin at different time interval.

### 3.2.4 Changes in amikacin antibiotic degradation efficiency at various ionic strength of the solution

Figure 11 illustrates the effect of ionic strength on amikacin degradation efficiency. At 0.02 M, poultry biowaste synthesized FeNPsachieved 47% degradation in the dark and 53% undersunlight, whereas *F. hispida* synthesized FeNPs showed 39% and 43%, respectively. When the ionic strength increased to 0.08 M, degradation efficiency by poultry biowaste FeNPs rose to 68% in the dark and 79% in sunlight, while *F. hispida* derived FeNPs reached 61% and 68%, respectively. The changes in degradation efficiencies with altering ionic strength are linked to electrolyte effect of FeNPssurface charge and aggregation. At low ionic strength (0.02 M), strong electrostatic repulsion ensures better dispersion and a larger surface area with both FeNPs showing good performance. However, sunlight providing a slight boost due to photocatalytic activity that enhances electron-hole pair generation. At 0.08 M, compression of the

electrical double layer reduced repulsion, promoting around the nanoparticles lowered repulsive forces, allowing them to aggregate more easily. This probably increased deterioration by boosting localized reactive species around contaminants, especially in the presence of light, rather than decreasing activity. FeNPs from poultry biowaste continuously performed better than those from F. hispida, presumably as a result of variations in surface functional groups, crystallinity, or electron-donating capacity [40]. At an ionic strength of 0.10 M, the efficiency was 74% in the dark and 89% in sunlight for poultry biowaste nanoparticles, whereas F. hispida nanoparticles achieved 66% in the dark and 73% in sunlight [41]. At 0.14 M, the efficiencies were 88% (dark)and 90% (sunlight) for poultry biowaste FeNPs, and 77% (dark) and 81% (sunlight) for F. hispida FeNPs.

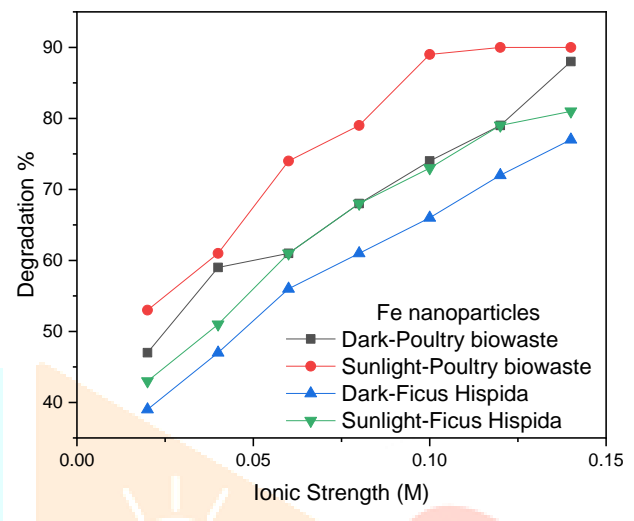


Figure 11. Variations in degradation efficiencies at different ionic strength.

# 3.2.5 Changes in amikacin antibiotic degradation efficiency at various pH of the solution

Figure 12 shows the effect of pH on amikacin antibiotic degradation efficiency. At pH 2, poultry biowaste derived FeNPs achieved 85% (dark) and 89% (sunlight), while F. hispida FeNPs showed 79% (dark) and 82% (sunlight). As the pH increased to 8, the efficiency was reduced to 71% (dark) and 73% (sunlight) for poultry biowaste FeNPs and 63% (dark) and 66% (sunlight) for F. hispida FeNPs[42]. At pH 10, the efficiency was further declined to 65% (dark) and 69% (sunlight) for poultry biowaste FeNPs and to 59% (dark) and 60% (sunlight) for F. hispida FeNPs[43]. The lowest performance was recorded at pH 14, where F. hispida FeNPs were 41% (dark) and 51% (sunlight) and poultry biowaste FeNPs were 53% (dark) and 59% (sunlight). FeNPs from poultry biowaste significantly outperformed those from F. hispida at all pH levels, and degradation was continuously accelerated by sunshine. Overall, acidic environments were found to have better efficiencies.

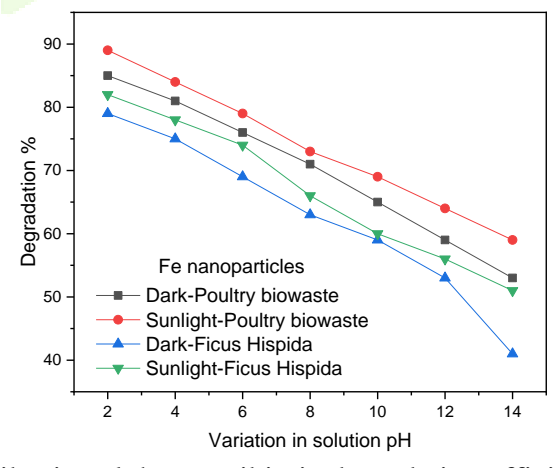


Figure 12. Variations in amikacin sulphate antibiotic degradation efficiency at various solution pH.

Amikacin breakdown using poultry waste derived FeNPs occurs mainly through adsorption. Their high surface area and reactivity enable the binding of amikacin molecules via electrostatic interactions, hydrogen bonding and Van der Waals interactions. This process reduces the concentration of amikacin in solution, thereby lowering its bioavailability. Instead of chemically breaking down the antibiotic, the nanoparticles immobilize it, reducing its toxicity and preventing further environmental pollution [44].

However, the F. hispida derived FeNPs contain functional groups including hydroxyl and carboxyl enable strong electrostatic interactions with amikacin, binding the antibiotic to the nanoparticle surface.

Using FeNPs from chicken biowaste and F. hispida bio-extract, amikacin is degraded via partial breakdown and adsorption. Amikacin is rendered immobile on the surface of the nanoparticles, and occasionally they produce reactive oxygen species (ROS) that break down its functional groups, reducing its toxicity and bioactivity to promote detoxification and stop environmental buildup.

# 3.3 Residual antibiotic activity studies

Residual antibiotic activity was evaluated using E. coli agar well diffusion method to determine the extent of antibiotic degradation. The degradation tests were conducted under standardized parameters: nanoparticle concentration of 1500 mg/l, amikacin concentration of 180 mg/l, reaction duration of 235 minutes, ionic strength of 0.08 M, and pH of 8. Four experimental setups were compared: poultry biowaste synthesized FeNPs in the dark, in sunlight, and F. hispida synthesized FeNPs in the dark, and in sunlight. The antibacterial assay revealed distinct variations in the inhibition zone diameters of E. coli following treatment with the two FeNPs systems. As shown in Figure 13, poultry biowaste-synthesized FeNPs produced comparatively smaller inhibition zones under both sunlight and dark conditions. This indicates that these nanoparticles increased degradation of the antibiotic, resulting in less residual activity in the medium [45]. Although inhibition zones under dark conditions were slightly larger than those under sunlight, the overall trend still pointed to efficient antibiotic removal by the poultry biowaste FeNPs (Figure 13).



After treated with poultry biowastesynthesized FeNPs -Dark



After treated with poultry biowastesynthesized FeNPs -Sunlight



After treated with F. hispida-synthesized FeNPs - Dark



After treated with F. hispida-synthesized FeNPs - Sunlight

Figure 13. Studies of residual antibiotic activity of Poultry biowaste-synthesized FeNPs and those of F. hispida- synthesized FeNPs under dark and light mode.

Moreover, FeNPs synthesized by F. hispida showed large inhibition zones both in the dark and light scenario, which indicates less adsorption and degradation of the antibiotic, and high degree of remaining activity. This variation underscores the greater efficacy of poultry biowaste-derived FeNPs in degrading the antibiotic compared with their F. hispida-derived counterparts, with light exposure further improving the degradation performance. Sunlight increases the production of reactive oxygen species (ROS), which speeds breakdown by converting complex antibiotic compounds into non-toxic metabolites [45]. F. hispida synthesized FeNPs had bigger inhibition zones as compared to poultry biowaste-derived FeNPs, indicating the role of capping agents in the surface chemistry, crystallinity, and/or catalytic characteristics. Moreover, both types of nanoparticles degraded better in sunlight highlighting the role of photocatalysis in enhancing ROS production. The considerably larger inhibition zones under dark settings highlight the significance of light-driven mechanisms in increasing degradation efficiency [46]. Overall, poultry biowaste synthesized FeNPs, exhibited more effective degradation of amikacin with the aid of light source, underscoring the need to incorporate light source (sunlight) in the degradation process.

#### IV. CONCLUSIONS

The work sought on the degradation of amikacin in pharmaceutical wastewater using FeNPs synthesized from poultry biowaste extract and *F. hispida* extract. UV-Vis and FT-IR spectroscopy confirmed the structural and functional characteristics of the synthesized FeNPs and antibiotic. Degradation tests were conducted under varied conditions, including different initial antibiotic and nanoparticle doses, reaction times, ionic strengths, and pH levels. The results showed that poultry biowaste derived FeNPshad higher degrading efficiency, particularly under sunlight compared to those synthesized from *F. hispida*. Poultry biowaste-derived FeNPs consistently achieved higher degradation rates under various conditions, demonstrating strong potential for antibiotic removal from simulated wastewater. The findings highlight the value of addition of bio-extracts to nanoparticles production and underscore the significant role of sunlight in enhancing the degradation process.

#### REFERENCES

- [1] Zhao, B., van Bodegom, P. M. and Trimbos, K. B. 2023. Antibiotic resistance genes in interconnected surface waters as affected by agricultural activities. *Biomolecules*, 13(2): 231.
- [2] Gwenzi, W., Simbanegavi, T. T. and Rzymski, P. 2023. Household disposal of pharmaceuticals in low-income settings: Practices, health hazards, and research needs. *Water*, 15(3): 476.
- [3] Manikandan, S. K., Pallavi, P., Shetty, K., Bhattacharjee, D., Giannakoudakis, D. A., Katsoyiannis, I. A. and Nair, V. 2023. Effective usage of biochar and microorganisms for the removal of heavy metal ions and pesticides. *Molecules*, 28(2): 719.
- [4] Kumari, S. and Das, S. 2023. Bacterial enzymatic degradation of recalcitrant organic pollutants: Catabolic pathways and genetic regulations. *Environmental Science and Pollution Research*, 30(33): 79676–79705.
- [5] Heris, S. Z., Etemadi, M., Mousavi, S. B., Mohammadpourfard, M. and Ramavandi, B. 2023. Preparation and characterizations of TiO<sub>2</sub>/ZnO nanohybrid and its application in photocatalytic degradation of tetracycline in wastewater. *Journal of Photochemistry and Photobiology A: Chemistry*, 443: 114893.
- [6] Khan, Z. U. H., Gul, N. S., Sabahat, S., Sun, J., Tahir, K., Shah, N. S. and Wu, J. 2023. Removal of organic pollutants through hydroxyl radical-based advanced oxidation processes. *Ecotoxicology and Environmental Safety*, 267: 115564.
- [7] Vinayagam, V., Palani, K. N., Ganesh, S., Rajesh, S., Akula, V. V., Avoodaiappan, R. and Pugazhendhi, A. 2023. Recent developments on advanced oxidation processes for degradation of pollutants from wastewater with focus on antibiotics and organic dyes. *Environmental Research*, 117500.
- [8] Khan, N., Kalsoom, F., Jamila, N., Shujah, S., Shah, A. U. H. A., Nishan, U. and Ullah, R. 2023. *Micromeria biflora* mediated gold and silver nanoparticles for colourimetric detection of antibiotics and dyes degradation. *Journal of King Saud University Science*, 35(11): 102999.
- [9] Sun, W., Wang, S., Yu, Z. and Cao, X. 2023. Characteristics and application of iron-based materials in heterogeneous Fenton oxidation for wastewater treatment: A review. *Environmental Science: Water Research & Technology*, 9(5): 1266–1289.
- [10] Alprol, A. E., Mansour, A. T., El-Beltagi, H. S. and Ashour, M. 2023. Algal extracts for green synthesis of zinc oxide nanoparticles: Promising approach for algae bioremediation. *Materials*, 16(7): 2819
- [11] Park, Y., Chakraborty, D. and Cho, E. B. 2024. Highly stable mesoporous Ni-phyllosilicate particle under high temperature hydrothermal and base conditions towards industrial catalytic applications. *Journal of Industrial and Engineering Chemistry*.
- [12] Dhiman, V. and Kondal, N. 2023. Bryophyllum pinnatum leaf extract mediated ZnO nanoparticles with prodigious potential for solar driven photocatalytic degradation of industrial contaminants. *Environmental Research*, 216: 114751.
- [13] Ahmadpour, N., Nowrouzi, M., Avargani, V. M., Sayadi, M. H. and Zendehboudi, S. 2024. Design and optimization of TiO<sub>2</sub>-based photocatalysts for efficient r
- emoval of pharmaceutical pollutants in water: Recent developments and challenges. *Journal of Water Process Engineering*, 57: 104597.
- [14] Priya, Naveen, Kaur, K. and Sidhu, A. K. 2021. Green synthesis: An eco-friendly route for the synthesis of iron oxide nanoparticles. *Frontiers in Nanotechnology*, 3: 655062.

- [15] Ashrafi, G., Nasrollahzadeh, M., Jaleh, B., Sajjadi, M. and Ghafuri, H. 2022. Biowaste- and nature-derived (nano) materials: Biosynthesis, stability and environmental applications. *Advances in Colloid and Interface Science*, 301: 102599.
- [16] Aguilar-Moreno, G. S., Navarro-Cerón, E., Velázquez-Hernández, A., Hernández-Eugenio, G., Aguilar-Méndez, M. Á. and Espinosa-Solares, T. 2020. Enhancing methane yield of chicken litter in anaerobic digestion using magnetite nanoparticles. *Renewable Energy*, 147: 204–213.
- [17] Thomas, L., Neelima, T. K. and Archana, T. M. 2024. From animal wastes and organic garbage waste to wealth A green approach. *Handbook of Advanced Biomass Materials for Environmental Remediation*, 43.
- [18] Zhang, Y., Wu, S. and Sun, P. 2023. Estimation of stability constants of Fe(III) with antibiotics and dissolved organic matter using a novel UV–vis spectroscopy method. *Science of The Total Environment*, 899: 165702.
- [19] Chapman, J., Orrell-Trigg, R., Kwoon, K. Y., Truong, V. K. and Cozzolino, D. 2021. A high-throughput and machine learning resistance monitoring system to determine the point of resistance for *Escherichia coli* with tetracycline: Combining UV-visible spectrophotometry with principal component analysis. *Biotechnology and Bioengineering*, 118(4): 1511–1519.
- [20] Al-Rufaie, M. M. M. and Motaweq, Z. Y. 2018. Estimation of Cephalosporins (Ceftriaxone, Ceftazidime) antibiotics as pure and pharmaceutic forms by color produced reaction in UV–Vis spectrophotometric technique. *Journal of Islamic Pharmacy*, 3(2): 1–15.
- [21] Hazra, K., Kumar, R., Sarkar, B. K., Chowdary, Y. A., Devgan, M. and Ramaiah, M. 2015. UV-visible spectrophotometric estimation of curcumin in nanoformulation. *International Journal of Pharmacognosy*, 2(3): 127–130.
- [22] Ali Talpur, M. M., Pirzada, T. and Arain, M. A. 2020. Application of UV-visible spectrophotometric method for the estimation of ciprofloxacin HCl and levofloxacin hemihydrate (antibiotics) in marketed drugs. *Journal of the Chemical Society of Pakistan*, 42(5).
- [23] Ashrafi, G., Nasrollahzadeh, M., Jaleh, B., Sajjadi, M. and Ghafuri, H. 2022. Biowaste- and nature-derived (nano) materials: Biosynthesis, stability and environmental applications. *Advances in Colloid and Interface Science*, 301: 102599.
- [24] Shah, S., Dasgupta, S., Chakraborty, M., Vadakkekara, R. and Hajoori, M. 2014. Green synthesis of iron nanoparticles using plant extracts. *International Journal of Biological and Pharmaceutical Research*, 5(7): 549–552.
- [25] Singh, P., Kim, Y. J., Zhang, D. and Yang, D. C. 2016. Biological synthesis of nanoparticles from plants and microorganisms. *Trends in Biotechnology*, 34(7): 588–599.
- [26] Giuntoli, J., De Jong, W., Arvelakis, S., Spliethoff, H. and Verkooijen, A. H. M. 2009. Quantitative and kinetic TG-FTIR study of biomass residue pyrolysis: Dry distiller's grains with solubles (DDGS) and chicken manure. *Journal of Analytical and Applied Pyrolysis*, 85(1–2): 301–312.
- [27] Chaudhary, S., Jain, V. P., Sharma, D. and Jaiswar, G. 2023. Implementation of agricultural waste for the synthesis of metal oxide nanoparticles: Its management, future opportunities and challenges. *Journal of Material Cycles and Waste Management*, 25(6): 3144–3160.
- [28] Ghaseminezhad, S. M., Hamedi, S. and Shojaosadati, S. A. 2012. Green synthesis of silver nanoparticles by a novel method: Comparative study of their properties. *Carbohydrate Polymers*, 89(2): 467–472.
- [29] Sadeghi, B. and Gholamhoseinpoor, F. 2015. A study on the stability and green synthesis of silver nanoparticles using *Ziziphora tenuior* (Zt) extract at room temperature. *Spectrochimica Acta Part A: Molecular and Biomolecular Spectroscopy*, 134: 310–315.
- [30] Dhaka, A., Mali, S. C., Sharma, S. and Trivedi, R. 2023. A review on biological synthesis of silver nanoparticles and their potential applications. *Results in Chemistry*, 101108.
- [31] Jalalah, M., Nayak, A. K. and Harraz, F. A. 2024. Eco-friendly preparation of nitrogen-doped porous carbon materials for enhanced solid-state supercapacitor device. *Diamond and Related Materials*, 111264.
- [32] Karunakaran, G., Cho, E. B., Kumar, G. S., Kolesnikov, E., Sudha, K. G., Mariyappan, K. and Choi, S. S. 2022. Citric acid-mediated microwave-hydrothermal synthesis of mesoporous F-doped HAp nanorods from biowaste for biocidal implant applications. *Nanomaterials*, 12(3): 315.
- [33] Saleem, M., Jamil, F., Qamar, O. A., Akhter, P., Hussain, M., Khurram, M. S. and Shah, N. S. 2022. Enhancing the catalytic activity of eggshell-derived CaO catalyst and its application in biodiesel production from waste chicken fat. *Catalysts*, 12(12): 1627.
- [34] Yasmin, S. R., Verma, Y. and Lawrence, R. 2021. Biowaste-derived nanoparticles and their preparation: A review. *The Scientific Temper*, 12(1&2).

- [35] Arularasu, M. V., Devakumar, J. and Rajendran, T. V. 2018. An innovative approach for green synthesis of iron oxide nanoparticles: Characterization and its photocatalytic activity. *Polyhedron*, 156:
- [36] Sorbiun, M., ShayeganMehr, E., Ramazani, A. and TaghaviFardood, S. 2018. Green synthesis of zinc oxide and copper oxide nanoparticles using aqueous extract of oak fruit hull (jaft) and comparing their photocatalytic degradation of basic violet 3. International Journal of Environmental Research, 12: 29–37.
- [37] Noor, N. N. M., Kamaruzaman, N. H., Al-Gheethi, A., Mohamed, R. M. S. R. and Hossain, M. S. 2023. Degradation of antibiotics in aquaculture wastewater by bio-nanoparticles: A critical review. Ain Shams Engineering Journal, 14(7): 101981.
- [38] Jayakrishnan, R., Joseph, A. and Thomas, V. 2021. Efficacy in degradation of carcinogenic pollutant sulforhodamine B by green synthesized silver nanoparticles. Micro and Nano Systems Letters, 9(1): 12.
- [39] Bazrafshan, E., Mohammadi, L., Zarei, A. A., Mosafer, J., Zafar, M. N. and Dargahi, A. 2023. Optimization of the photocatalytic degradation of phenol using superparamagnetic iron oxide (Fe<sub>3</sub>O<sub>4</sub>) nanoparticles in aqueous solutions. RSC Advances, 13(36): 25408–25424.
- [40] Jarvin, M., Kumar, S. A., Rosaline, D. R., Foletto, E. L., Dotto, G. L. and Inbanathan, S. S. R. 2022. Remarkable sunlight-driven photocatalytic performance of Ag-doped ZnO nanoparticles prepared by green synthesis for degradation of emerging pollutants in water. Environmental Science and Pollution Research, 29(38): 57330-57344.
- [41] French, R. A., Jacobson, A. R., Kim, B., Isley, S. L., Penn, R. L. and Baveye, P. C. 2009. Influence of ionic strength, pH, and cation valence on aggregation kinetics of titanium dioxide nanoparticles. Environmental Science & Technology, 43(5): 1354–1359.
- [42] Gilani, S. A. B., Naseeb, F., Kiran, A., Ihsan, M. U., Iqbal, J., Javed, H. M. A. and ShabirMahr, M. 2024. pH dependent synthesis of ceria nanoparticles for efficient sunlight-driven photocatalysis of methyl orange containing wastewater. Optical Materials, 148: 114871.
- [43] Wang, C. T. 2007. Photocatalytic activity of nanoparticle gold/iron oxide aerogels for azo dye degradation. Journal of Non-Crystalline Solids, 353(11–12): 1126–1133.
- [44] Mora-Gamboa, M. P., Rincón-Gamboa, S. M., Ardila-Leal, L. D., Poutou-Piñales, R. A., Pedroza-Rodríguez, A. M. and Quevedo-Hidalgo, B. E. 2022. Impact of antibiotics as waste, physical, chemical, and enzymatical degradation: Use of laccases. *Molecules*, 27(14): 4436.
- [45] Rajiygandhi, G. N., Maruthupandy, M., Li, J. L., Dong, L., Alharbi, N. S., Kadaikunnan, S. and Li, W. J. 2020. Photocatalytic reduction and antibacterial activity of biosynthesized silver nanoparticles against multidrug-resistant Staphylococcus saprophyticus BDUMS 5 (MN310601). Materials Science and Engineering: C, 114: 111024.
- [46] Mühling, M., Bradford, A., Readman, J. W., Somerfield, P. J. and Handy, R. D. 2009. An investigation into the effects of silver nanoparticles on antibiotic resistance of naturally occurring bacteria in an estuarine sediment. Marine Environmental Research, 68(5): 278–283.